

RCNN with Swallow Swarm Optimization for Liver Disease Detection and Classification

N Nanda Prakash

Department of E.C.E.,
Koneru Lakshmaiah Education Foundation,
Vaddeswaram 522302, India
le-mail: nandaprakashnelaturi@gmail.com

V Rajesh

Department of E.C.E.,
Koneru Lakshmaiah Education Foundation,
Vaddeswaram 522302, India
e-mail: rajesh4444@kluniversity.in

Syed Inthiyaz

Department of E.C.E.,
Koneru Lakshmaiah Education Foundation,
Vaddeswaram 522302, India
e-mail: syedinthiyaz@kluniversity.in

Abstract— One of the most serious medical conditions that can endanger a person's life and health is liver disease. The second-leading cause of death for men and sixth-leading cause of death for women, respectively, is liver cancer. In 2008, liver cancer claimed the lives of almost 750,000 people, killing 960,000 of them. The segmentation and identification of CT images produced by computer tomography has emerged as a major topic in medical image processing. There are few choices for liver segmentation due to the enormous amount of time and resources necessary to train a deep learning model. As part of this research, we created the Region utilizing Convolutional Neural Network, a novel way of extracting the liver from CT scan images (RCNN). The suggested CNN approach, which employs softmax to isolate the liver from the background, contains of three convolutional layers and two entirely associated layers. In the CapsNet and CAL layers, there are class dependencies and an efficient mechanism to connect CAL and subsequent CapsNet processing. Finally, the classification is carried out using the SSO-CSAE model, an approach known as the swallow swarm optimization that is based on the Convolutional Sparse Autoencoder (CSAE) The MICCAI SLiver '07, 3Dircadb01, and LiTS17 benchmark datasets were used to validate the proposed RCNN-SSO approach. When compared to other frameworks, the proposed framework performed well in numerous categories.

Keywords- Region with Convolutional Neural Network (RCNN), focal liver lesions, detection, classification, computed tomography, swallow swarm optimization (SSO).

I. INTRODUCTION

The liver is a crucial organ that weighs about 1.5 kg and makes up roughly 2% of the body's overall weight. The liver is necessary for the body to be able to maintain itself. Hepatic sinusoids and hepatocytes make up the liver histologically, and each has a specific physiological purpose. The liver is referred to as the body's "chemical factory". More than two-thirds of the acute hepatitis cases in the world are found in this region, according to a WHO analysis. According to a WHO study, cirrhosis is the foremost reason of liver disease-related deaths in Asia. According to the CDC, over 399,000 people died in 2016 from cirrhosis, hepatocellular carcinoma, and hepatitis C (CDC). According to the World Health Organization, hepatitis C is a public health hazard (WHO).

Several epidemiological studies and risk factors over the previous numerous decades have shown that hepatitis C and liver sores are widespread and can be fatal. Blood infections, stomach infections, infections caused by injuries, and bacterial or parasitic infections are the most common causes of liver sores.

In order to avoid future issues, those suffering from abscesses should be informed of their severity, diagnosis, and treatment. Pyogenic liver abscesses are a common cause of pyogenic liver abscesses. A variety of causes can contribute to liver disease. Damaged cells are unable to recover after a certain point, resulting in irreparable injury. The liver may develop fibrosis, scar tissue, or dysfunctional liver cells. Cirrhosis and liver fibrosis were considered incurable conditions in the 1970s. Cirrhosis, according to Laennec in 1819, was a primary liver malignancy that could be identified by its colour. Fibrosis in the liver can progress to cirrhosis, the last stage of fibrosis in which the liver is damaged, enlarged, and non-functioning cells form abnormally. When a liver tumour is secondary, more individuals will discover it than a primary liver tumour. The majority of metastatic liver cancer is still contained within the liver in 70 to 80 percent of patients. Liver metastases are frequently underexposed in unenhanced CT images. If hepatic steatosis is present, the lesions may be solitary or somewhat hyperattenuated. A texture is made up of a blend of uniform and different patterns or frequencies. The statistical properties of

texture, on the other hand, are more quantifiable. The texture of the liver has a similar characteristic. The texture of the inside of a liver and its borders with other organs may make it hard to tell the difference between abnormal and healthy tissue.

The databases Web of Science, Google Scholar, PubMed, and EMBASE were used to find relevant literature on liver disease diagnosis. We looked for phrases like "machine learning," "texture analysis," "computed tomography," "computer-aided diagnosis," "computer-aided diagnostic," and others. We discovered just a few datasets and approaches in our early study on the issue, so we created our personal dataset of approximately 3000 CT scans, which is the research's chief influence. Several important works on the subject are mentioned in the bibliography.

Utilizing an a priori probability map of the liver, the 3D CNN technique was able to provide the initial liver surface for automated liver segmentation. This was accomplished through the use of a prior knowledge. This model makes use of both local and global data, and it does so based on the segmentation that came before it. For the research of the unhealthy liver, local nonparametric information is utilised, whereas for the study of the healthy liver, global nonparametric information is utilised. In order to overcome the challenge of liver segmentation, convolutional neural networks were put to use. In terms of discrimination and optimization, the 3D-DSN model provided by 1e outperforms the CNN model. The 3D-DSN prototypical, a fully convolutional learning prototypical, is used in this situation. In this work, deep supervision of the hidden layer was applied to enhance the optimization convergence rate and precision. In post-processing, the segmentation is fine-tuned via a conditional random field. When it came to segmenting the liver and its tumors, Octave CNN was proven to be superior. Cancers on CT images may be reliably diagnosed using deep learning algorithms. As seen above, CFCNN was qualified on the 3D CT capacity of the liver and then utilized to excerpt the liver and its graze from CT data slices, as seen above. Following that, the segmentation results are enhanced by 3D-CRF post-processing. Models of completely 3D convolutional neural networks demand additional parameters, memory, and computing power. Instead of employing the whole three-D CNN system, these plane covers are used for segmentation. As a result, because 3-dimensional convolutional neural networks (CNN) are more computationally costly and need a longer training time than 2-dimensional models, their use is discouraged. Over segmentation may develop as a result of bias in a limited number of groups.

For simplicity's sake, we employed a 2D convolutional neural network rather than a fully 3D CNN for handling the data. Some form of preprocessing is necessary to generate a higher-quality CT image. A CNN is fed two-dimensional patches to build the probability map.

1. To detect the liver in CT scan images, convolutional neural networks (CNN) are utilized.

2. A three-layer RCNN model with convolutional and fully linked layers is proposed.

3. A random Gaussian distribution is used to establish the weights, and this distribution ensures that the information distance is preserved.

4. To increase data adaptability, each convolutional layer was followed by an LRN layer. SLiver '07, 3Dircadb01, and LiTS17 are four 1-ree benchmark datasets that we use to analyze and recover the presentation of our prototypical.

The remainder of the paper is structured as follows: In Unit 2, a review of the works is given. In Unit 3, classification, techniques, and the CNN structure are talked about. In Section 4, the results of the experiments are talked about, and in Section 5, a conclusion is given.

II. LITERATURE SURVEY

The researchers, Ben-Cohen et al. [1], built fully convolutional networks for the identification of liver and lesion cells. The FCN is being investigated using a small dataset and patch-based CNN classification methods. They have CT images of 20 people on a single slice, each having a smallest of 67 lesions and 42 livers; they also have 3D segmented livers from 22 patients. Cross-validation results reveal that the FCN outperforms all of its competitors. Our completely automated method yielded optimistic charges of 0.85 and 0.7 false positives per instance, which is incredibly encouraging and therapeutically helpful.

ML experts S. Muthuselvan and his colleagues [2] investigated a variety of potential machine learning models, including SVM, neural networks, decision trees, and others. In this section of the study, classification systems for liver disease are analysed and discussed. The algorithms random tree (RT), J48, and K-star were utilised in this study. There were a variety of classification strategies utilised, including logistic regression, RT, and SVM. In order to estimate liver disease data, XGBoost was utilised, and the authors referred to L1 and L2 throughout. To overcome an imbalance in ILPD, the minority oversampling strategy was applied. The performance of balanced and imbalanced datasets was evaluated using SVM and KNN.

[3] proposed the Watershed Transform and Gaussian Mixture Model (WT-GMM) to identify liver cancer using deep learning.

The detection accuracy of this technique is built on the Gaussian blend model and the marker-controlled watershed transformation. The approach given is tested using real-time clinical data from many individuals. Automatic identification achieved a precision of 99.38 percent with almost no authentication loss using a deep-neural system classifier. The DNN model may be used as a first stage in the detection process to detect liver tumors. The proposed strategy is evaluated for clinical and decision-making reasons by employing an effectual methodology to detect the site of tumor on liver CT images. The volume of the lesion must be known, which can be done by putting together different photo slices into a mesh.

C. Han et al. [4] used 3D multi-conditional GAN to naturally place realistic heterogeneous lung nodules in CT scans with the goal of enhancing lung nodule discovery compassion in CT imageries. This was done in instruction to increase the sensitivity of lung nodule identification in CT scans (MCGAN). When compared to a fixed false positive rate, the detection findings acquired by the 3D CNN always performed better than those obtained by other approaches, regardless of how large or small the nodule was (FPR). MCGAN's lung nodules are an excellent technique to sidestep a lack of medical data.

Linguraru et al. [5] employed generic-affinity invariant shape parameterization and the geodesic-active outline technique to segment a liver tumor. According to Li and colleagues [6], the superficial of the liver may be recognized using a graph cut with a form restraint. Rusku et al. [7] used CT images to divide the 3D liver via neighborhood-connected region growth. Level set techniques are utilized to successfully

segment the liver because they can capture intricate shapes while controlling shape regularity. A picture can show both local and global information with a sparse representation.

Histological images were used by I. Hirra et al. [8] to categorize chest tumor using a deep belief network. A stacked auto encoder is used to record the high-level structures of the 1e skin. A CNN is a common deep learning technique for visual object recognition and nonlinear mapping detection. In this study, we examine the grouping of Mask R-CNN and GANs to segment multimodal newborn brain pictures and enhance pixel-wise classification performance. Previous research has proposed similar ways. Scientists created synthetic medical pictures using generative adversarial networks (GANs) to assist CNNs in improving their classification performance on actual medical images. This is made feasible by the use of computer-generated medical imaging.

L. Chen et al. [10-12] presented the dense res-induction network, an enhanced convolution layer for learning the features of medical images (DRINET). [13-16] A more accurate and explainable medical picture segmentation system was constructed by Gu and colleagues with the help of attention-based CNN. This system is conscious of the most pertinent spatial locations, channels, and scales all at the same time. [17-20]. Chinese researchers made an MRF-CNN for segmenting liver portal regions in Hematoxylin and Eosin (H&E) stained whole-slide pictures (WSIs).

In a unique technique, Yu et al. [21,22] used ultrasonic resonance largeness and deep learning to assess liver fibrosis. Both of these properties were considered by the algorithm. This approach classifies computer simulation results as either normal or fibrosis tissue [23-26]. The information can be classified in two ways. Reddy et al. [27-31] introduced a novel CAD system based on convolution neural networks and transfer learning. Here's a fun fact: (pre-trained VGG-16 model).

III. PROPOSED SYSTEM

Our goal is to assess whether an MR image of the liver reveals anything benign or malignant. The three components of our RCNN-SSO technique are depicted in Figure 1: Data visualization and evaluation at numerous levels and scales, including multiple representation scales and levels. Figure 1: The Organization This section contains information about these three sections.

A. Preparation of the data

In the planned experiment, respectively axial CT slice is preprocessed. We were able to find an information range of 0 to 1 thanks to improved contrast and zero mean and unit alteration normalization of the dataset. The training and testing datasets were created in the same manner. We went one step further and upgraded the input data for the training dataset. Cut the training data to remove the liver slices, then rotate the pictures at 90, 180, and 270 degrees. Statistics increase is lengthily studied in the works. To generate both training and testing data, 1.3 million random patches were chosen at random from a pool of 32 different axial 2D pictures. For reliable training and validation, one picture patch from each of two classes is used in a 1:1 ratio.

The block diagram of the proposed RCNN-SCO method clearly explains its process. The first stage is known as the preprocessing stage, and it is important to note that data preprocessing is a component of data preparation. Data preprocessing refers to any type of processing that is performed

on raw data in order to get it ready for another data processing operation. For many years, this has served as one of the process of data mining's most significant preliminary steps. Different parameters like ALB, AST, ALP, ALT, AST, GGT, CREA, and PROT are used in disease prediction. The RCNN-SSO algorithm is used to figure out if a disease test report is positive or negative.

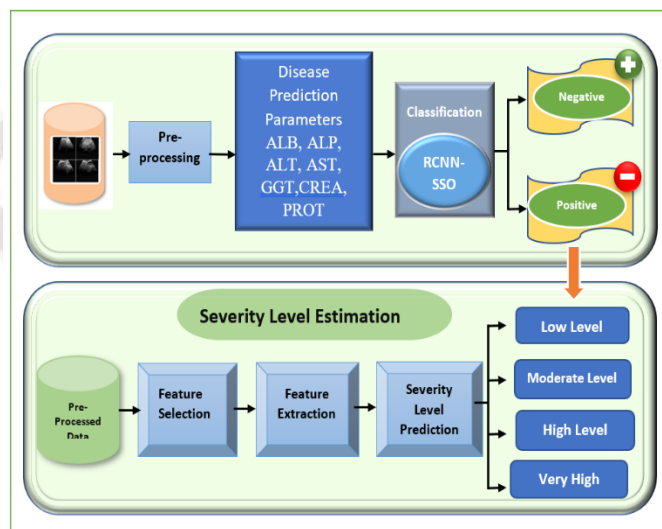


Figure 1. Proposed Diagram of RCNN-SSO

The next module is the severity level estimation, where the depth of the disease is checked and monitored. The different steps carried out in this phase are preprocessing, feature selection, feature extraction, and severity level prediction. The process of turning unprocessed raw data into numerical features that may be processed while preserving the accuracy of the data in the original data set is known as feature extraction. The data from the initial data set can still be used after doing this. One of the very first steps in the process of developing a predictive model is feature selection, which refers to the repetition of reducing the number of input variables as much as possible. It is desired to restrict the number of variables that are input into the model in order to improve the performance of the model and, in some cases, to reduce the amount of computing that is required for the modelling process. The severity is categorized under the following four different categories, namely low, moderate, high, and very high.

B. Representation at Multiple Scales

We employ MR images of liver lesions as input in our research on a patch-based diagnostic paradigm. We suggest using a multiscale sampling strategy in order to abstract complementing feature information that is both local and semi-local in scale. In our study experiments, three patch sizes (large, intermediate, and tiny) were employed (256x256, 128x128 and 64x64 voxels) (Figure 2). For each lesion in the MR picture, cropping at trio distinct scales was performed.

We decided to utilise a recurrent convolutional neural network (RCNN) to train globally discriminative feature representations from image patches because deep learning models perform so well. In order to accurately represent the scales, three RCNNs were trained with patch data taken from the respective training scales. In our testing, our method is applicable to any RCNN structure, including the self-defined

RCNN structure as well as commonly used conventional RCNN structures such as Resnet, VGG, or Alexnet. This is the case regardless of whether the RCNN structure is self-defined or not. These three RCNNs could be trained using a variety of approaches, incorporating transfer learning or not, or even none of these approaches. Transfer learning may be used to aid the training process for a network with a large number of parameters and minimal training data. Albert Comelli et al. and Renato Cuocolo et al. discovered that lightweight networks like Enet can be trained from scratch without the need for transfer learning. In our transfer learning tests, we employed the technique and widely used large-scale networks. Before we fine-tuned the CNNs, we taught each one with a large set of pictures, like the ones in the ImageNet database [48], which we used in our research.

input and output, respectively. The output of the nth layer may be calculated using the following equation.

$$C_q^{(m)} = F_{w,b}(\sum_p C_p^{n-1} * W_{p,q}^n, b_q^n) \quad (1)$$

The bias of the jth output record in this convolutional layer is given by, which is the convolution's denotation. suggests a non-linear activation function. Nonlinear activation methods include sigmoid, hyperbolic tangent, and rectified linear unit activation. A sub-sampling layer is placed after the convolutional layer to further reduce calculations. As a consequence, we may employ the normal maximum pool layer in a novel manner. A SoftMax classifier sorts the output after convolutional layers and before fully connected ones. It is used to normalize the kernel convolution consequences in binary organization difficulties. Convolutional layers may distribute their weights more effectively when using CNN. The same filter is applied to all of the pixels in the layer. The key advantage is a reduction in memory use while still enhancing performance.

The training set has m labelled samples.

$\{(x^1, y^1), (x^2, y^2), \dots, (x^m, y^m)\}$, y^p can be 0 or 1, where $I = (1, 2, 3, \dots, m)$

We can learn all we need to know about the RCNN by looking at the parameters. The following cost function is reduced for logistic regression.

$$E(0) = -\frac{1}{m} [\sum_{p=1}^m y^p \log F_\theta(x^p) + (1 - y^p) \log(1 - F_\theta(x^p))] \quad (2)$$

The higher values in the SoftMax layer can be punished by weight decay while doing classification regularization. The cost function may be minimized using gradient-based optimization, and the partial derivatives can be calculated via back propagation.

F. Swallow Swarm Optimization (SSO) Algorithm

This novel technique to optimization is inspired by the primary notion of the swallow swarm. This algorithm's particles are classified into three types:

1. The explorer particle (e_i)
2. Particle with no apparent direction of travel (O_i)
3. A leading particle (l_i)

These particles are continually in touch with one another and travel in a traditional route. Individually particle in a group (which may contain numerous sub-colonies) has a role in directing the colony to a better state of things.

1) Particle of the Explorer

This subpopulation constitutes the vast majority of the colony's members. They are responsible for doing research into the problem space. If a particle has reached an extreme point in problem space (such as swallowing) and then utilizes a specific sound to steer the group, it can act as a head leader. If a subdivision is in a better (but not the best) position than its neighbors, it is selected as the local leader; otherwise, each particle's (velocity vector of element toward HL), (velocity

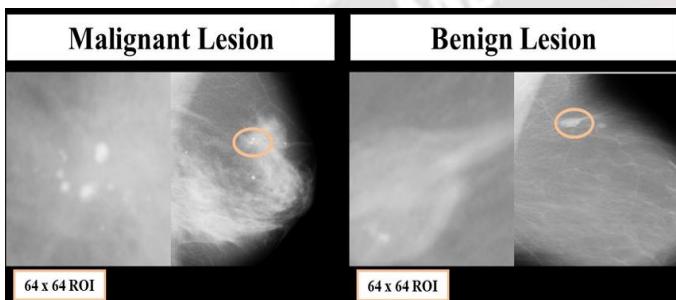


Figure 2 Instances of benign and malignant lesions

The output of the RCNN's feature extractor was utilized to create a feature vector for each patch. A CT scan of a lesion revealed three feature vectors for each of the three scales. As an extra bonus, the last layer of each RCNN gave a binary diagnostic of the patch on a comparable scale. As a result, each RCNN must be classified independently.

C. The Multi-Level Fusion Method

We combined data at the feature and decision levels in order to make use of multi-scale complementary property data and improve organizational robustness.

D. Fusion at the Feature Level

The property data of a lesion might change based on the size of the patch. The three patch scales were integrated using three layers of neural networks. The first step was to integrate three separate patch-scale feature vectors. Lastly, we ran our function in two layers that were linked to each other and made the fused feature diagnostic. These photos were used to try out different settings for a three-layer neural network, which were then used to give the network random values.

E. A RCNN-olutional neural network is used to create a region of interest

The convolutional neural network is the topic of this section (RCNN). The 1e RCNN is based on a multilayer perception discrepancy. RCNN is built on convolutional and subsampling layers. Convolutional neural networks consist of numerous convolutional layers that are stacked on top of one another. These layers are used for feature learning. A convolutional system's layers may all access the preceding layer's feature map. These layers are related to some filters. For the n convolutional layers, we use I as the feature map of the nth layer and I as its

vector of element toward LL), and capability of their subsequent path make a chance transfer. Figure 3 displays a particle's passage through the problem domain.

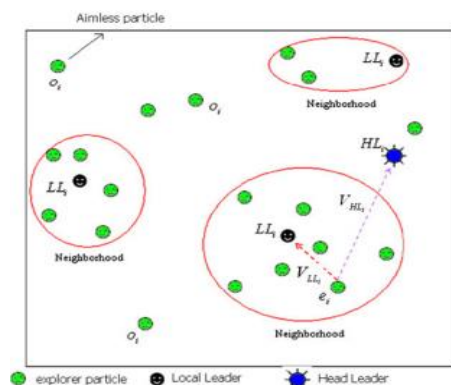


Figure 3 Three types of particles and how they move.

The behavior of explorer particles is greatly influenced by their vector [1]. The particle's current position in the problem space represents its most recent and stable position. Because it has the highest likelihood of reacting in its current location, this particle is a leader particle. The aHL and bHL coefficients are used to adjust the acceleration in an adaptive way. Both of these properties are influenced by the element's movement. If the subdivision is at a smallest opinion (minimalizing difficulty), using a minimal number of control coefficients is advised, and it should be recognized that the particle may be at a global minimum at this time. If the particle's position is better than but less than average, it should go toward If the subdivision's location is inferior than, it is therefore feasible to move further. Keep in mind that the vector has an effect on this movement.

2) Aimless particle

These particles' starting location with regard to other particles is poor, as is the quantity of $f(o_i)$ they have. These particles are isolated from traveler elements and assigned a new job in the collection after being recognized (o_i). They are responsible for performing an investigative and ad hoc exploration. When they jump touching at random, it has nothing to do with where they are. The swallows' job is to explore new areas and report backbone to the break of the colony if they discovery anything interesting. Many optimization problems have a local optimum. This is because the ideal solution is concealed from the group's view when particles are arranged incorrectly in position space. This is the most challenging aspect of optimization issues (early convergence in the optimal pints for the immediate area). Examine the opportunity of disregarding the global perfect response, travelling to various neighboring locations with their huge hops, and investigate the optimization scenario for particles o_i , which appear to have aimless behaviour. The particle o_i utilizes the local optimum points to find its exact placement.

While looking for the best location, it will swap seats with the adjacent traveler element, but if it doesn't, it will continue. To get the new location of each particle in o_i , divide one-to-two-thirds of the random number in position space by a number between one and two. The division answer is created at random from particle o_i 's prior location.

Rosen rock functions can be used to cover a large range of values (-50, 50). With rand (minimum, maximum), we obtain 25, and using rand (26), we get 0, giving us a fractional number of 12.5. As a consequence, by adding or removing this amount, the value of o_i may now be changed. Having additional alternatives allows you to investigate more of the surroundings.

3) The leader particle

The SSO algorithm employs particles known as "leaders." At the start of the search for positions in position space, these particles have the lowest $f(l_i)$. The position and number of them may change depending on the level. PSO has a single leader particle, but this new approach may also contain one. Particles of this kind can be found spread across the cosmos or clumped together in a concentrated location. The best leader in the colony is known as the Leader Head, while some particles are known as Local Leaders. Candidates for good responses that we will keep In the current world, there are several smaller swallow colonies, each with thousands of members. The leadership of these sub-colonies periodically changes owing to the wisdom and power of other swallows. The bird who has the best position in terms of food and resting locations in a flock of swallows is termed the "leader," which is why they are nicknamed "leaders." It is the leader's responsibility to direct the remainder of the colony to this spot. This problem is simulated using the SSO approach. If an aimless particle discovers a place in each repeat where the best answer to the problem has been found thus far, it can act as a leader particle. Because of the quick and dynamic nature of swallow migrations, true boundaries between sub-colonies may never be formed. The size of the sub-colonies will determine how the plan for the swallows and how many of them there will be.

It is possible for each of these three particles (e_i, O_i and l_i) to fulfil any of these three functions at any one time. Even though these particles' roles may shift repeatedly during the search, locating the optimal spot remains the most critical objective.

IV. RESULT AND EVALUATION

1) Experimental Setup

During the training of the neural network, around sixty contrast-enhanced CT imageries were working. For the purpose of this investigation, we made use of the SLiver '07 exercise set, the 3Dircadb01 exercise dataset, and the LiTS17 training dataset. We made fantastic use of each and every one of them. CT scans from the SLiver '07, 3Dircadb01, and LiTS datasets were used for training and validation, with ten pictures from each set. Entirely trio standard datasets are easily accessible connected. For testing, 30 CT pictures with an axial slice resolve of 512 512 pixels were chosen. For each of the three datasets (SLiver'07, 3Dircadb01, and LiTS17), 10 CT scans were chosen at random. MATLAB 2021 was used to implement the model for the experiments. For the settings of this experiment, Stochastic Gradient Descent with Momentum, a beginning knowledge amount of 0.01 was employed (SGDM). On the used PC, Microsoft Windows, an Intel Core i-7, 8565U CPU, 32GB of RAM, and a 2GB GPU (NVIDIA GeForce 250) were all loaded.

When we applied our technique, we physically reset the masses with a Gaussian distribution with a normal eccentricity of 0.0001. In this study, we used a Gaussian-weighted RCNN network to connect the model's output properties to the input data. We eventually got our model to function well after 70 iterations and a knowledge amount of 0.01. The education rate released by 0.1 after 20 repetitions. The momentum was kept constant at 0.9 throughout the research. The decay amount was 0.0001 and the sample size was 64. The stochastic gradient descent technique is used in the SGD with momentum optimization approach. When the surface curvature is much narrower in one dimension than the other, SGD 1 e encounters difficulty. Methods for generating momentum are critical to the SGD's success. The key parameters for the training programme are shown in Tables 3 and 4. Several critical modules that influence and extract patches examine the predicted model performance. Figure 5 displays the trio convolutional layers of the training prototypical.

The initial liver probability map is employed as a starting point for the trained RCNN algorithm in an iterative procedure. The iterative conclusions of the liver-colored probability map for one of the test capacity are depicted in figure 6. The liver becomes brighter at the eighth and fifteenth iterations, implying that the liver pixels are stronger and more distinct. As in previous iterations, the spleen continues to decrease in the 25th edition. After 35 tries, the spleen and liver were finally removed. Between iterations 60 and 70, validation results are similar, and the shape of the liver is shown correctly.

2) *Assessment criteria*

When we predicted, something was going to happen, and it did, it's known as a True Positive (TP)

True Negatives (TN): The occurrence that we expected to be false and the actual yield was also false.

There were instances in which we expected something to be true, but it turned out to be incorrect.

Negative results (FN): the event that we expected to be true but ended up being true anyway.

$$\text{Precision} = \frac{TP}{TP + FP} \tag{3}$$

$$\text{Recall} = \frac{TP}{TP + FN} \tag{4}$$

$$\text{F1-Score} = \frac{2TP}{2TP + FP + FN} \tag{5}$$

$$\text{Accuracy} = \frac{TP + TN}{TP + TN + FP + FN} \tag{6}$$

3) *Precision*

TABLE 1. PRECISION ANALYSIS

Impact of precision analysis (%)					
Dataset	CNN	DNN	SVM	ANN	RCNN-SSO
SLiver'07	87.48	89.69	93.03	92.65	93.34
3Dircadb01	89.22	91.25	93.48	94.83	95.73
LiTS17	93.26	92.37	94.24	95.17	96.62

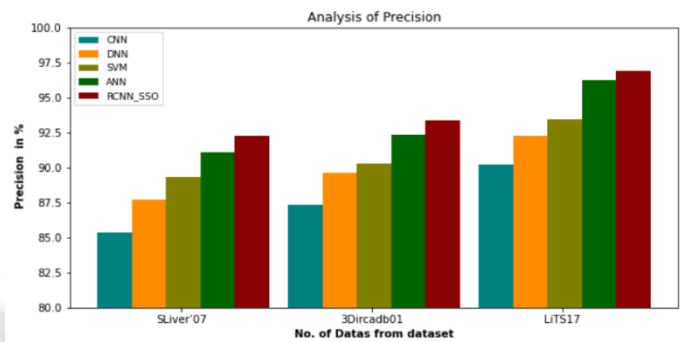


Figure.4. Analysis of precision with Existing methods

Figure.4 and Table.1 exhibit the results of the RCCN-SSO model's thorough liver disease classifications and identified methodologies. CT images are used to segment the liver, and three hard datasets used for this task are 3Dircadb01, LiTs17, and SLiver'07. We demonstrate that with segmentation of datasets, we compare the current system to the suggested technique in precision analysis. The recommended values of the proposed system are greater than those of current systems. The precision of RCCN-SSO under SLivet'07, 3Dircadb01, and LiTS17 datasets is 93.34%, 95.73%, and 96.62%. The precisions of CNN, DNN, SVM, and ANN methods using the dataset SLivet'07 are 87.48%, 89.69%, 93.03%, and 92.65% respectively. Under dataset 3Dircadb01 dataset, the precision for CNN, DNN, SVM, and ANN was 89.22%, 91.25%, 93.48%, and 94.83%, respectively. Similarly, with the LiTS17 dataset, the precision for CNN, DNN, SVM, and ANN is 93.26%, 92.37%, 94.24%, and 95.17%, respectively.

4) *Recall*

TABLE.2 RECALL ANALYSIS

Impact of precision analysis (%)					
Dataset	CNN	DNN	SVM	ANN	RCNN-SSO
SLiver'07	88.36	87.72	98.35	91.13	92.24
3Dircadb01	91.24	89.61	90.31	92.36	93.36
LiTS17	90.24	95.24	93.45	96.04	96.94

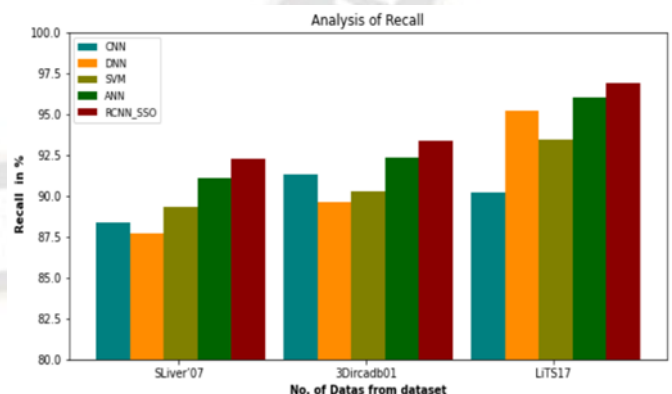


Figure.5. Analysis of Recall with Existing methods

Table.2 and Figure.5 exhibit the results of the RCCN-SSO model's thorough liver disease classifications identified methodologies. CT images are used to segment the liver, and three hard datasets used for this task are 3Dircadb01, LiTs17, and SLiver'07. We demonstrate that with segmentation of datasets, we compare the current system to the suggested

technique in recall analysis. The recommended values of the proposed system are greater than those of current systems. The recall of RCCN-SSO under SLiver'07, 3Dircadb01, and LiTS17 datasets is 92.24%, 93.36%, and 96.94%. The recall of CNN, DNN, SVM, and ANN methods using the dataset SLiver'07 is 88.36%, 87.72%, 98.35%, and 91.13%, respectively. Under dataset 3Dircadb01 dataset, the recall for CNN, DNN, SVM, and ANN was 91.24%, 89.61%, 90.31%, and 92.36%, respectively. Similarly, with the LiTS17 dataset, the recall for CNN, DNN, SVM, and ANN is 90.24%, 95.24%, 93.45%, and 96.04%, respectively.

5) F1-Score

TABLE.3 F-SCORE ANALYSIS

Dataset	No of Data from dataset	CNN	DNN	SVM	ANN	RCNN-SSO
SILVER'07	100	82.26	85.17	87.43	89.55	91.24
	300	83.26	86.72	88.26	90.47	92.34
	500	84.26	87.34	89.16	91.32	93.11
3DIRCADB01	100	84.16	86.33	88.16	90.47	92.45
	300	83.17	85.25	86.56	89.63	93.53
	500	82.25	88.52	89.36	91.24	94.22
LiTS17	100	85.26	87.17	89.16	91.28	93.41
	300	89.31	90.17	91.16	92.26	94.35
	500	83.41	85.26	85.16	89.18	95.22

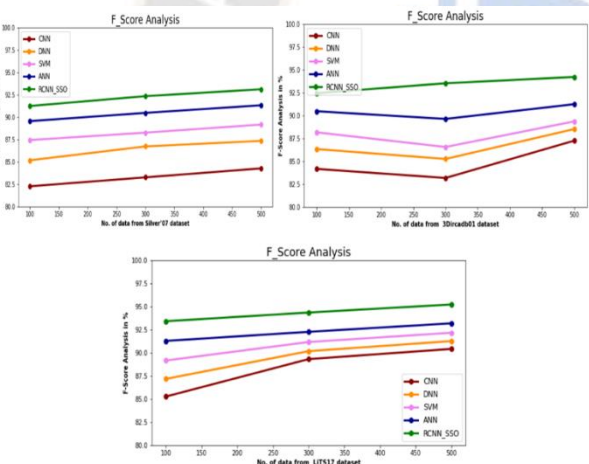


Figure.6 Analysis of F-Score with Existing methods

Table 3 and Figure 6 show the F-score study of the RCNN-SSO technique with present methods below different datasets. The F-score value of RCCN-SSO under SLiver'07, 3Dircadb01, and LiTS17 datasets is 93.11%, 94.22%, and 95.22 % for 500 data whereas the F-score values of CNN, DNN, SVM, and ANN methods using the dataset SLiver'07 is 84.26%, 87.34%, 89.16%, and 91.32%, respectively and it is 82.25%, 88.52%, 89.36% and 91.24% under 3Dircadb01 dataset respectively and the F-score values under LiTS17 dataset is 83.41%, 85.26%, 85.16% and 89.18% respectively.

6) Accuracy

Figure.7 and Table.4 exhibit the results of the RCNN-SSO model's thorough liver disease classifications and identified methodologies. CT images are used to segment the liver, and three hard datasets used for this task are 3Dircadb01, LiTs17, and SLiver'07. We demonstrate that with segmentation of datasets, we compare the current system to the suggested technique in accuracy analysis. The recommended values of the

proposed system are greater than those of current systems. The accuracy of RCCN-SSO under SLiver'07, 3Dircadb01, and LiTS17 datasets is 93.80%, 95.71%, and 96.60%. The accuracy of CNN, DNN, SVM, and ANN methods using the dataset SLiver'07 is 87.43%, 89.64%, 93.01%, and 92.61%, respectively. Under the dataset 3Dircadb01 dataset, the accuracy for CNN, DNN, SVM, and ANN was 91.90%, 91.22%, 93.43%, and 94.81%, respectively. Similarly, with the LiTS17 dataset, the accuracy for CNN, DNN, SVM, and ANN is 93.26%, 92.33%, 94.22%, and 95.14%, respectively.

TABLE.4 ACCURACY ANALYSIS

Impact of Accuracy analysis (%)					
Dataset	CNN	DNN	SVM	ANN	RCNN-SSO
SLIVER'07	87.43	89.64	93.01	92.61	93.80
3DIRCADB01	91.90	91.22	93.43	94.81	95.71
LiTS17	93.26	92.33	94.22	95.14	96.60

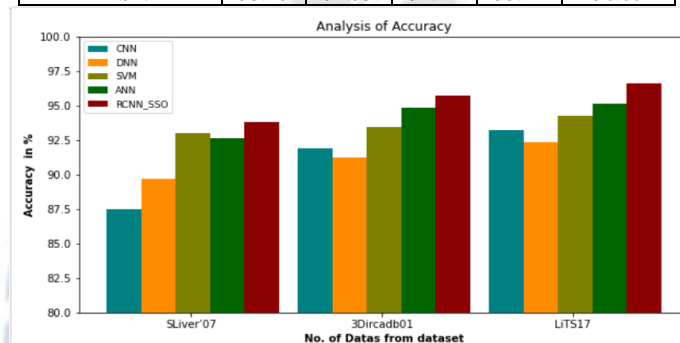


Figure.7 Analysis of accuracy with Existing methods

V. CONCLUSION

This work proposes combining CNNs at many scales and levels to utilize RCNN-SSO, an explainable deep learning technique, to differentiate benign from malignant liver lesions in CT images. The multi-level fusion diagnostic method needs to be built in order to complement feature descriptions, it was obvious to analyses abrasion on three different patch sizes, each of which was a different size. We created an efficient classifier by combining information at the feature-level, as well as the decision-level, in order to take advantage of courtesy data from three distinct patch sizes. This study goes into great detail about the diagnostic performance difference as well as the decision-making process. The visual qualities accounted for the disparities in diagnostic performance. The depiction of the attention map improved the decision-making process. To put our strategy to the test, we employed a variety of RCNN architectures. When compared to a single-scale technique, the testing findings revealed that while feature fusion improved performance, multi-level fusion improved it much more. The feature and decision-level fusion of the RCNN-SSO method was shown to be substantial.

Future studies will look at the relative benefits of various training methods, including but not limited to transfer learning. We intend to acquire CT scans from other patients and conduct additional external validation to advance our study. The addition of an attention mechanism to our diagnostic model will increase diagnosis accuracy even further. By experimenting with fresh ways of describing and visualizing deep learning models, the

objective is to make the liver diagnosis model more transparent to users. Displaying hidden layers, neurons, and gradients are examples of these tactics.

REFERENCES

- [1] A. Ben-Cohen, I. K. E. Diamant, M. Amitai, and H. Greenspan, "Fully convolutional network for liver segmentation and lesions detection," in *Deep Learning and Data Labeling for Medical Applications*. Cham, Switzerland: Springer, 2016, pp. 77–85.
- [2] Muthuselvan, S.; Rajapraksh, S.; Somasundaram, K.; Karthik, K. Classification of Liver Patient Dataset Using Machine Learning Algorithms. *Int. J. Eng. Technol.* 2018, 7, 323–326. [CrossRef] .
- [3] A. Das, U. R. Acharya, S. S. Panda, and S. Sabut, "Deep learning based liver cancer detection using watershed transform and Gaussian mixture model techniques," *Cognit. Syst. Res.*, vol. 54, pp. 165–175, May 2019.
- [4] C. Han, Y. Kitamura, A. Kudo et al., "Synthesizing diverse lung nodules wherever massively: 3D multi-conditional GANbased CT image augmentation for object detection," in *2019 International Conference on 3D Vision (3DV)*, Quebec City, QC, Canada, 2019.
- [5] M. G. Linguraru, W. J. Richbourg, J. M. Watt, V. Pamulapati, and R. M. Summers, "Liver and tumor segmentation and analysis from CT of diseased patients via a generic affine invariant shape parameterization and graph cuts," in *Proceedings of the International MICCAI Workshop on Computational and Clinical Challenges in Abdominal Imaging*, pp. 198–206, Bethesda, MD, USA, September 2011.
- [6] G. Li, X. Chen, F. Shi, W. Zhu, J. Tian, and D. Xiang, "Automatic liver segmentation based on shape constraints and deformable graph cut in CT images," *IEEE Transactions on Image Processing*, vol. 24, no. 12, pp. 5315–5329, 2015.
- [7] L. Ruskó, G. Bekes, and M. Fidrich, "Automatic segmentation of the liver from multi- and single-phase contrast-enhanced CT images," *Medical Image Analysis*, vol. 13, no. 6, pp. 871–882, 2009.
- [8] I. Hirra, M. Ahmad, A. Hussain et al., "Breast cancer classification from histopathological images using patch-based deep learning modeling," *IEEE Access*, vol. 9, pp. 24273–24287, 2021.
- [9] M. Frid-Adar, I. Diamant, E. Klang, M. Amitai, J. Goldberger, and H. Greenspan, "GAN-based synthetic medical image augmentation for increased CNN performance in liver lesion classification," *Neurocomputing*, vol. 321, pp. 321–331, 2018.
- [10] L. Chen, P. Bentley, K. Mori, K. Misawa, M. Fujiwara, and D. Rueckert, "DRINet for medical image segmentation," *IEEE Transactions on Medical Imaging*, vol. 37, no. 11, pp. 2453–2462, 2018.
- [11] R. Gu, G. Wang, T. Song et al., "CA-net: comprehensive attention convolutional neural networks for explainable medical image segmentation," *IEEE Transactions on Medical Imaging*, vol. 40, no. 2, pp. 699–711, 2021.
- [12] Q.-E. Xiao, P.-C. Chung, H.-W. Tsai et al., "Hematoxylin and eosin (H & E) stained liver portal area segmentation using multi-scale receptive field convolutional neural network," *IEEE Journal on Emerging and Selected Topics in Circuits and Systems*, vol. 9, no. 4, pp. 623–634, 2019.
- [13] Y. Yu, J. Wang, C. W. Ng et al., "Deep learning enables automated scoring of liver fibrosis stages," *Scientific Reports*, vol. 8, no. 1, p. 16016, 2018.
- [14] D. S. Reddy, R. Bharath, and P. Rajalakshmi, "A novel computer-aided diagnosis framework using deep learning for classification of fatty liver disease in ultrasound imaging," in *Proceedings of the 2018 IEEE 20th International Conference on e-Health Networking, Applications and Services (Healthcom)*, Ostrava, Czech Republic, September 2018.
- [15] Byra M, Styczynski G, Szmigielski C, Kalinowski P, Michałowski Ł, Paluszkiwicz R, Ziarkiewicz-Wróbiewska B, Zieniewicz K, Sobieraj P, Nowicki A (2018) Transfer learning with deep convolutional neural network for liver steatosis assessment in ultrasound images. *Int J Comput Assist RadiolSurg* 13(12).
- [16] K. He, X. Liu, R. Shahzad et al., "Advanced deep learning approach to automatically segment malignant tumors and ablation zone in the liver with contrast-enhanced CT," *Frontiers in Oncology*, vol. 11, p. 2735, 2021.
- [17] Y. A. Ayalew, K. A. Fante, and M. A. Mohammed, "Modified U-Net for liver cancer segmentation from computed tomography images with a new class balancing method," *BMC Biomedical Engineering*, vol. 3, no. 1, pp. 1–13, 2021.
- [18] Akhondi, H.; Sabih, D. Liver Abscess. 2021. Available online: <https://www.ncbi.nlm.nih.gov/books/NBK538230/> (accessed on 15 October 2021).
- [19] Pere, G.; Graupera, I.; Lammert, F.; Angeli, P.; Caballeria, L. Screening for liver fibrosis in the general population: A call for action. *Lancet Gastroenterol. Hepatol.* 2016, 1, 236–264.
- [20] Siriwardena, K.; Mason, J.M.; Mullamitha, S.; Hancock, H.C.; Jegatheswaran, S. Management of colorectal cancer presenting with synchronous liver metastases. *Nat. Rev. Clin. Oncol.* 2014, 8, 446–459. [PubMed]
- [21] 13. Azer, S.A. Deep learning with convolutional neural networks for identification of liver masses and hepatocellular carcinoma: A systematic review. *World J. Gastrointest. Oncol.* 2019, 12, 1218–1230.
- [22] Xu, J.; Jing, M.; Wang, S.; Yang, C.; Chen, X. A review of medical image detection for cancers in digestive system based on artificial intelligence. *Expert Rev. Med. Devices* 2019, 10, 877–889.
- [23] Nayantara, P.V.; Kamath, S.; Manjunath, K.; Rajagopal, K. Computer-aided diagnosis of liver lesions using CT images: A systematic review. *Comput. Biol. Med.* 2020, 3, 234–248.
- [24] M. Nasr, M. M. Islam, S. Shehata, F. Karray, and Y. Quintana, "Smart healthcare in the age of AI: recent advances, challenges, and future prospects," *IEEE Access*, vol. 9, 2021.
- [25] M. Z. Islam, M. M. Islam, and A. Asraf, "A combined deep CNN-LSTM network for the detection of novel coronavirus (COVID-19) using X-ray images," *Informatics in Medicine Unlocked*, vol. 20, Article ID 100412, 2020.
- [26] L. J. Muhammad, M. M. Islam, S. S. Usman, and S. I. Ayon, "Predictive data mining models for novel coronavirus (COVID-19) infected patients' recovery," *SN Computer Science*, vol. 1, no. 4, pp. 206–207, 2020.
- [27] A. Asraf, M. Z. Islam, M. R. Haque, and M. M. Islam, "Deep learning applications to combat novel coronavirus (COVID19) pandemic," *SN Computer Science*, vol. 1, no. 6, pp. 363–367, 2020.
- [28] P. Saha, M. S. Sadi, and M. M. Islam, "EMCNet: automated COVID-19 diagnosis from X-ray images using convolutional neural network and ensemble of machine learning classifiers," *Informatics in Medicine Unlocked*, vol. 22, Article ID 100505, 2021.
- [29] M. Ahmad, D. Ai, G. Xie et al., "Deep belief network modeling for automatic liver segmentation," *IEEE Access*, vol. 7, pp. 20585–20595, 2019.
- [30] Nanda Prakash, N, Rajesh V., Inthiyaz, Syed, "An uncertain Liver Segmentation in Computed Tomography Images with Enhanced generative Mask Region on CNN" *Int. J. Intell. Syst. Appl. Eng.* 2022, 10, 2, 184–190.
- [31] Murty, S.V.; Kumar, R.K. Accurate Liver Disease Prediction with Extreme Gradient Boosting. *Int. Eng. Adv. Technol.* 2019, 8, 2288–229